Journal of Power Sources 202 (2012) 175–183

Contents lists available at SciVerse ScienceDirect

Journal of Power Sources

journal homepage: www.elsevier.com/locate/jpowsour

# Lattice Boltzmann simulations of liquid droplets development and interaction in a gas channel of a proton exchange membrane fuel cell

Bo Han, Ji Yu, Hua Meng*

*School of Aeronautics and Astronautics, Zhejiang University, Hangzhou, Zhejiang 310027, China*

ARTICLE INFO

*Article history:*
Received 11 October 2011
Received in revised form
25 November 2011
Accepted 25 November 2011
Available online 6 December 2011

*Keywords:*
Lattice Boltzmann model
Fuel cell
Gas channel
Two-phase flows
Liquid droplet interaction

ABSTRACT

Liquid water transport in gas channels may influence and even prevent gas supply in a proton exchange membrane (PEM) fuel cell, so significantly affect cell operation. A two-phase two-dimensional lattice Boltzmann model is employed in this paper to simulate the development and interaction of two liquid droplets in a gas channel of a PEM fuel cell, focusing mainly on parametric effects, including the gas flow velocity, initial droplet distance, different micropore combinations, and the gas diffusion layer (GDL) surface wetting properties, on liquid droplet transport behaviors. Results confirm that an increased gas stream velocity and liquid pore distance may prevent liquid droplet interaction and enhance liquid water removal. Numerical simulations further indicate that different pore size combinations may promote droplet interaction, particularly with a large pore in front of a small one. On the contrary, a more hydrophobic GDL surface can decrease liquid droplet interaction, benefit liquid water removal, and consequently improve PEM fuel cell water management.



## 1. Introduction

Liquid water transport and distribution is a paramount issue in proton exchange membrane (PEM) fuel cell water management and plays a dictating role in fuel cell performance and durability. In the past decade, many experimental [1–10] and numerical studies [11–31] have been conducted in this area to elucidate the fundamental liquid water transport mechanisms and their effects on fuel cell operation. In recent years, to obtain deeper insight into the underlying physics, the lattice Boltzmann method has also been employed for direct numerical simulations of liquid water transport in porous materials of PEM fuel cells with realistic micropore structures [32–35]. These meso-scale studies paint a clearer picture of liquid water transport process in PEM fuel cells with physical details not attainable using current experimental techniques.

Although good progress has been achieved in numerical modeling of liquid water transport in the porous materials in PEM fuel cells, there still remains a weak area concerning liquid water dynamic behaviors in gas channels. Liquid water transport in gas channels may influence and even prevent gas supply in a PEM fuel cell and thus significantly affect fuel cell operation. No comprehensive and robust numerical model capable of accurately handling liquid water transport in the gas channels of a PEM fuel cell exists in the open literature. So far, almost all the available PEM fuel cell models treat liquid water transport in a gas channel as a mist flow, which assumes tiny liquid droplets moving synchronously with the gas stream. The mist flow model can only cover a very small portion of the liquid water transport regions in the gas channels of PEM fuel cells.

Given the practical importance of liquid water transport behaviors in PEM fuel cell gas channels, many experimental studies have been carried out to lay a foundation for fundamental understanding of the phenomena [1–3]. Yang et al. built an optically transparent PEM fuel cell to observe liquid water transport processes in the cathode gas channel [2]. It was found that liquid water droplets could emerge from the gas diffusion layer (GDL) interior to its channel surface at preferential locations, with droplet diameters ranging from a few to hundreds of micrometers. These liquid droplets would subsequently grow and interact on the GDL surface, and under certain operation conditions, could block gas flow and cause possible cell operation shut-down. Zhang et al. [3] further studied liquid water removal phenomena in the cathode gas channel using a similar transparent fuel cell. The experimental results revealed two major modes of liquid water removal from the GDL surface; one being droplet detachment by the shear forces of gas flow, which subsequently led to a mist flow in the gas channel, and the other being capillary wicking of liquid droplets onto the hydrophilic channel walls, which resulted in the annular film flow and/or liquid slug flow.

To obtain more physical insights, a number of numerical simulations have been further performed to study liquid water transport mechanisms in PEM fuel cell gas channels. Quan et al.

* Corresponding author. Tel.: +86 571 87952990.
*E-mail address:* menghua@zju.edu.cn (H. Meng).

0378-7753/$ – see front matter © 2011 Elsevier B.V. All rights reserved.
doi:10.1016/j.jpowsour.2011.11.071

**Nomenclature**

| | |
|---|---|
| $c$ | lattice space and time ratio |
| $c_s$ | lattice speed of sound |
| $\vec{e}$ | lattice velocity vector |
| $f$ | density distribution function |
| $\vec{F}$ | external force |
| $\vec{F}_{ads}$ | adhesive force |
| $\vec{F}_{\text{int}}$ | inter-particle force |
| $\vec{F}_g$ | body force |
| $G$ | constant controlling interaction strength |
| $P$ | pressure |
| $\Delta P$ | pressure difference, Pa |
| $r$ | droplet radius, m |
| $R$ | gas constant |
| $s$ | index function |
| $T$ | temperature |
| $t$ | time |
| $\vec{u}$ | macroscopic fluid velocity vector |
| $u_g$ | inlet gas stream velocity, m s$^{-1}$ |
| $\vec{x}$ | space position vector |

*Greek symbols*

| | |
|---|---|
| $\theta$ | contact angle |
| $\rho$ | fluid density |
| $\rho_0$ | constant density |
| $\rho_w$ | tunable parameter |
| $\sigma$ | surface tension, N m$^{-1}$ |
| $\tau$ | relaxation time |
| $\omega_\alpha$ | weighting factor |
| $\psi$ | potential function |
| $\psi_0$ | constant |

*Superscripts*

| | |
|---|---|
| $eq$ | equilibrium |

*Subscripts*

| | |
|---|---|
| $\alpha$ | direction index |
| $g$ | gas phase |
| int | inter-particle parameter |

[36] investigated liquid water droplet behaviors and interaction with the air stream and channel walls in a serpentine gas channel of a PEM fuel cell. The volume of fluid (VOF) method was applied to track the liquid water surface. Numerical results indicated that the bend area of the serpentine channel would exert significant influences on the air flow and liquid water transport and distribution inside the channel. It was found that under specific operation conditions, liquid water flooding might block the gas channel and prevent reactant supply. The same method has later been employed by this research group to study liquid water transport in straight parallel channels with the inlet and outlet manifolds in a PEM fuel cell stack [37]. Recently, Hao and Cheng [38] used the lattice Boltzmann method to simulate liquid water droplet dynamic behaviors on a hydrophobic GDL surface. The detailed process of a liquid water droplet emerging from a micropore in the GDL, its continuous growth on the GDL surface, and the final detachment from the micropore was clearly presented. It was concluded that the gas flow velocity and GDL surface wetting properties would strongly affect the liquid droplet movement. This research work also demonstrated that the lattice Boltzmann method could be a powerful tool for numerical simulations of liquid water transport phenomena in the gas channels of PEM fuel cells.

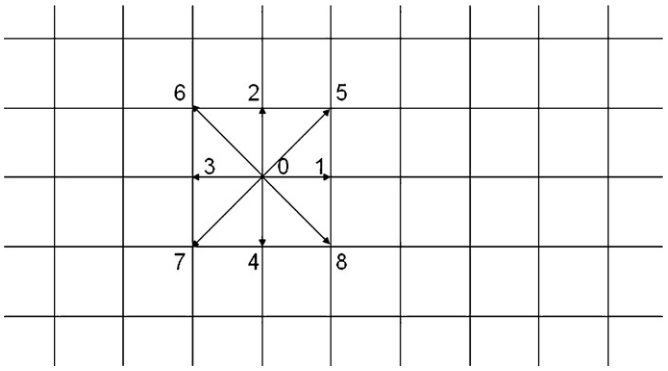


**Fig. 1.** Schematic of the D2Q9 scheme, showing fixed lattices in a 2D space and 9 specified particle streaming directions (including a stationary one).

In this paper, a two-phase two-dimensional lattice Boltzmann model is employed for direct numerical simulations of the emergence, growth, and subsequent interaction of two liquid water droplets on the GDL surface in a gas channel of a PEM fuel cell. Particular attention has been paid to the effects of a number of key influential parameters on liquid water droplets development and interaction, including the gas flow velocity, initial droplet distance, different micropore combinations, and the GDL surface wetting properties. The simulation results may help to gain more fundamental insights on liquid water dynamic behaviors in PEM fuel cell gas channels.

## 2. Theoretical formulation

In this paper, we implemented a lattice Boltzmann model (LBM) in a two-dimensional configuration to simulate liquid droplets development and interaction in a gas channel of a PEM fuel cell. LBM is a powerful and convenient tool for simulating multi-phase flows, since it can maintain phase interface automatically during numerical calculation without resorting to more complicated interface tracking techniques commonly used in the conventional numerical methods for multi-phase simulations, as in the VOF approach. The lattice Boltzmann method simulates fluid flows through the evolution of the particle density distribution functions on fixed lattices. The calculations proceed in two steps: collision and streaming. The collision procedure relaxes the density distribution functions on a lattice toward the equilibrium states, while the streaming step moves the particle distributions to the immediate neighboring lattices with specified velocity magnitudes and directions. A number of different multi-phase LBM approaches have been proposed and have been successfully applied in many fluid flow simulations [39–44], including liquid water transport in the porous materials of PEM fuel cells [32–35].

The present numerical calculations are based on the lattice Boltzmann method with a single relaxation time collision operator (the so-called LBGK model) and the popular D2Q9 scheme, as shown in Fig. 1. The Shan-Chen multi-phase model is further implemented for studying two-phase liquid droplets development and interaction [39,40,43]. The lattice Boltzmann equation can be expressed as

$$f_\alpha(\vec{x}+\vec{e_\alpha}\Delta t, t+\Delta t) = f_\alpha(\vec{x}, t) - \frac{\Delta t}{\tau}(f_\alpha(\vec{x}, t) - f_\alpha^{eq}(\vec{x}, t)) \quad (1)$$

where $f$ is the density distribution function, $x$ refers to space position, $t$ time, $\alpha$ the velocity direction, and $\tau$ the relaxation time. It should be emphasized that the lattice Boltzmann model is formulated and solved in dimensionless form, so the relevant parameters in this model are all dimensionless ones without units [39,40,44].

In Eq. (1), the equilibrium distribution function is calculated as

$$f_\alpha^{eq}(\vec{x},t) = \omega_\alpha \rho \left[1 + \frac{\vec{e_\alpha}\cdot\vec{u^{eq}}}{c_s^2} + \frac{(\vec{e_\alpha}\cdot\vec{u^{eq}})^2}{2c_s^4} - \frac{(\vec{u^{eq}})^2}{2c_s^2}\right] \quad (2)$$

In Eq. (2), $\rho = \sum_\alpha f_\alpha$ is the fluid density. In the D2Q9 scheme, the weighting factor, $w_\alpha$, is chosen to be 4/9 for $\alpha = 0$, 1/9 for $\alpha = (1, 2, 3, 4)$, and 1/36 for $\alpha = (5, 6, 7, 8)$ to fully recover the Navier–Stokes equation [44]. The parameter, $e_\alpha$, represents the 9 discrete velocities, as shown in Fig. 1, and are defined as

$$\left[\vec{e_0}, \vec{e_1}, \vec{e_2}, \vec{e_3}, \vec{e_4}, \vec{e_5}, \vec{e_6}, \vec{e_7}, \vec{e_8}\right] = c \cdot \begin{bmatrix} 0 & 1 & 0 & -1 & 0 & 1 & -1 & -1 & 1 \\ 0 & 0 & 1 & 0 & -1 & 1 & 1 & -1 & -1 \end{bmatrix} \quad (3)$$

where $c = \Delta x/\Delta t$ is the ratio between the lattice space distance and time step. The parameter, $c_s$ in Eq. (2), is given as $c/\sqrt{3}$ in the LBGK model [44]. In this dimensionless LBGK simulation, $\Delta x$ and $\Delta t$ are both set to be unity.

In the Shan-Chen model [39,40], extra forces have been introduced to account for fluid inter-particle and fluid–solid interactions. These forces are incorporated into the equilibrium velocity as

$$\vec{u^{eq}} = \vec{u'} + \frac{\tau \vec{F}}{\rho} \quad (4)$$

where the macroscopic velocity is

$$u' = \frac{\sum_\alpha f_\alpha e_\alpha}{\rho} \quad (5)$$

The extra forces in Eq. (4) is defined as

$$\vec{F} = \vec{F_{\text{int}}} + \vec{F_{ads}} + \vec{F_g} \quad (6)$$

In Eq. (6), the parameter, $\vec{F_g}$, represents a uniform steady body force. The inter-particle cohesive force is introduced as follows:

$$\vec{F_{\text{int}}}(\vec{x},t) = -G\psi(\vec{x},t)\sum_\alpha \omega_\alpha \psi(\vec{x} + \vec{e_\alpha}\Delta t, t)\vec{e_\alpha} \quad (7)$$

where $G$ is a constant representing the interaction strength between neighboring particles, while the weighting factor $\omega_\alpha$ has the same values as in Eq. (2). The parameter, $\psi$, is a density-dependent potential function given as

$$\psi(\rho) = \psi_0 \exp\left(\frac{-\rho_0}{\rho}\right) \quad (8)$$

where the parameters, $\psi_0$ and $\rho_0$, are two constants.

In this study, the following equation of state, which allows for liquid–gas phase coexistence, is applied:

$$P = \rho RT + \frac{GRT}{2}\psi^2(\rho) \quad (9)$$

where the dimensionless parameter, $RT$, is equal to 1/3, according to the gas kinetic theory [41].

The parameters, $G$, $\psi_0$, and $\rho_0$, are chosen to be −125, 4, and 200, respectively, based on previous two-phase studies using the LBGK model [40,41] and our requirement for large gas and liquid density ratio in the present simulation.

In Eq. (6), an adsorption force is also included to account for liquid and solid phase interactions, which is formulated as

$$\vec{F_{ads}}(\vec{x},t) = -G\psi(\rho(\vec{x},t))\sum_\alpha \omega_\alpha \psi(\rho_w)s(\vec{x} + \vec{e_\alpha}\Delta t, t)\vec{e_\alpha} \quad (10)$$

where $s$ is an index function with a value of 1 if the site at $\vec{x} + e_\alpha \Delta t$ is in solid phase, with a value of 0 otherwise. $\rho_w$ is a free parameter for tuning different wall properties, e.g. the contact angle.

More details concerning this two-phase lattice Boltzmann model can be found in the open literature [39–44].

## 3. Model validation

The two-phase lattice Boltzmann model briefly described in the last section has been programmed into a computational software package in our group and validated herein using two test cases. The first test case concerns liquid–gas interaction and phase separation, which would lead to surface tension. Fig. 2 shows many liquid droplets with different diameters obtained after conducting phase separation calculation. The results provide necessary information for determining the surface tension. According to the Laplace equation, the following formula exists:

$$\Delta P = \frac{\sigma}{r} \quad (11)$$

which basically states that the pressure difference, $\Delta P$, inside and outside a droplet is proportional to the surface tension, $\sigma$, and inversely proportional to the droplet radius, $r$.

Using the results in Fig. 2, the droplet surface tension can be calculated using pressure differences and droplet radii, and the calculated results are presented in Fig. 3. The surface tension obtained from the present LBM approach agrees very well with the Laplace equation, as clearly verified in Fig. 3.

The second test case concerns liquid–solid interaction, which would lead to different wetting characteristics of a solid surface, e.g. different contact angles as illustrated in Fig. 4. By changing the parameter, $\rho_w$, in Eq. (10), the strength of liquid and solid interactions can be varied in the present two-phase LBM approach. This naturally results in different solid surface contact angles, as illustrated in Fig. 5, which shows a liquid droplet in contact with a solid wall under different wetting conditions.

The numerical results obtained in the two test cases clearly indicate that the two-phase lattice Boltzmann model presented in the last section is capable of handling liquid–gas and liquid–solid interactions. Therefore, it is suitable for simulating liquid droplets development and interaction in a gas channel in a PEM fuel cell.

It should be noted that because of the lack of high-resolution experimental data in both time and space concerning the following two droplets interaction in the gas channel of a PEM fuel cell, model validation in this paper is conducted against two representative two-phase phenomena. Although this is a common practice and has been proven to be a reliable approach [34,38–44], direct validation using high-resolution experimental data can

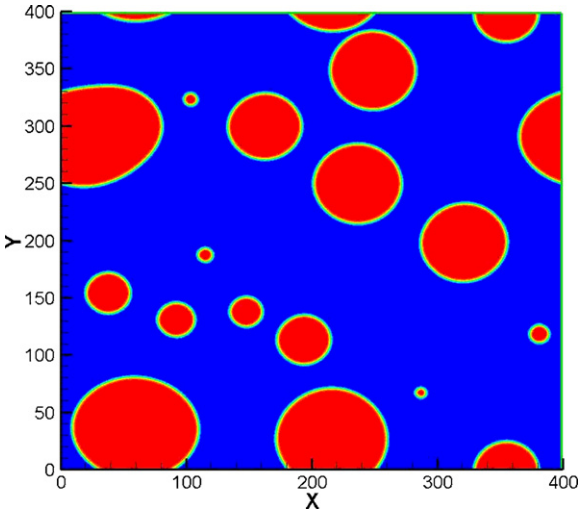


**Fig. 2.** Liquid droplets with different diameters after a phase separation calculation.

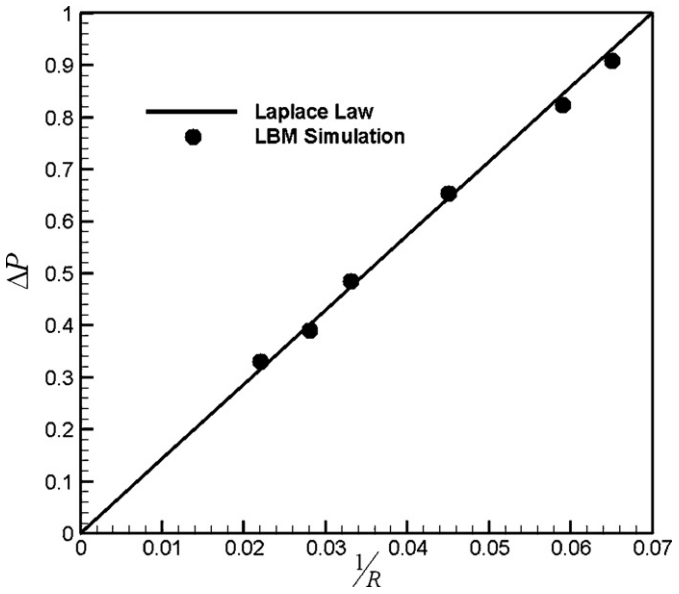


**Fig. 3.** Comparisons of the calculated surface tension with Laplace equation.

provide further confidence and should be carried out once the experimental data become available.

## 4. Results and discussion

A two-phase two-dimensional lattice Boltzmann model has been presented and validated in the earlier sections, and is employed here to study liquid droplet development and interaction in a gas channel of a PEM fuel cell, as illustrated in Fig. 6. Previous experimental results [2,3] have clearly illuminated that liquid droplets would emerge, move, and interact on the GDL surface in the PEM fuel cell gas channel. The present numerical studies are intended to provide more details on liquid droplet interaction processes and help enhancing fundamental understanding of the dynamic phenomena. The present LBM simulations focus mainly on the effects of various key parameters, including the gas stream velocity, micropore size and distance, and GDL surface wetting properties, on liquid droplet transport behaviors.

As shown in Fig. 6, the gas channel depth is chosen to be 500 μm, and its length is 1000 μm. There are two micropores in the GDL on one side of the channel, with the pore width chosen as 30 μm unless otherwise specified. These are representative parameters for a typical PEM fuel cell. In the simulations, liquid water is forced into the gas channel through the two micropores with a specified inlet velocity of 0.08 m s$^{-1}$ [38]. Gas stream flows into the gas channel with a parabolic shape, assuming a fully developed laminar flow. The GDL surface contact angle is specified at 120°. Based on grid independence studies, 500 × 250 regular lattices are placed in the gas channel region in the $x$ and $y$ directions, respectively, while 15 × 50 lattices are used in each of the micropores.

In the following LBM simulations, effects of the inlet gas stream velocity on droplet interactions are first investigated. In this part of simulations, the distance between the two micropores are specified at 240 μm, while the averaged inlet gas stream velocity varies from 2.0 to 4.0 m s$^{-1}$.

The transient variations of the two liquid droplets transport are displayed in Fig. 7. The movement of the two droplets is mainly influenced by the shear force from the gas stream, droplet surface tension, and two droplets interaction. As shown in Fig. 7, with a low inlet gas velocity at 2.0 m s$^{-1}$, the two droplets emerging from the micropores would be slightly elongated along the flow direction, but neither of them could be pulled away from the pores under the relatively weak shear drag. Eventually, the leading droplet would grow sufficiently large to merge with the trailing droplet, forming a single large deforming droplet under the influence of the shear force. The existence of this large droplet would further affect the gas stream velocity distribution, as shown in Fig. 8.

As the inlet gas velocity is increased to 3.0 m s$^{-1}$, the two emerging droplets would exhibit different interaction behaviors. As the shear drag acting on the leading droplet becomes stronger, this

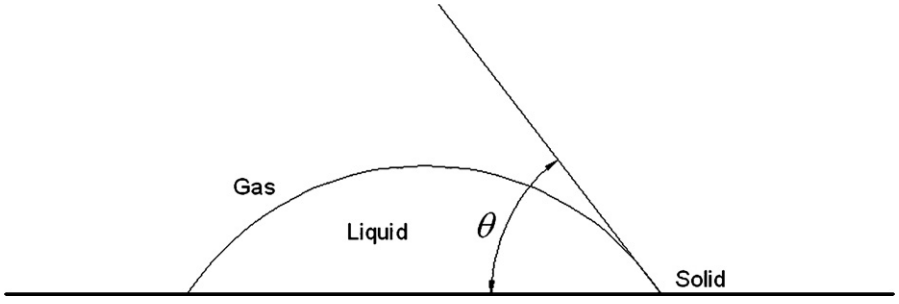


**Fig. 4.** Interaction of a liquid droplet with a solid surface and the contact angle definition.

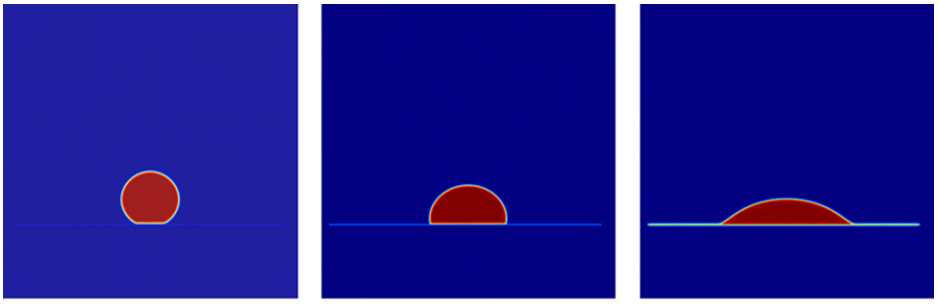


**Fig. 5.** Liquid droplet attached to a solid wall at different contact angles.

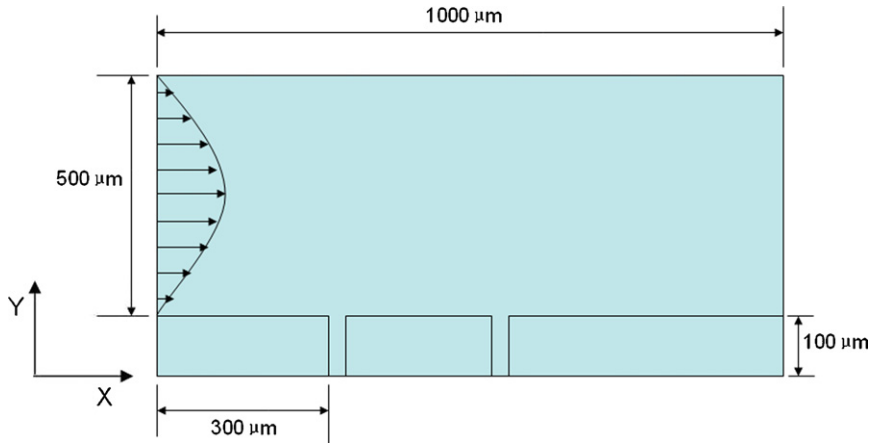


**Fig. 6.** Physical configuration for numerical simulations of liquid droplets interaction.

droplet is detached from its feeding pore and subsequently collides with the trailing droplet. The liquid water region formed by the two droplets exhibits a quite flat shape under the strong gas stream shear force. As shown in Fig. 7, once the inlet gas stream velocity is further increased to 4.0 m $s^{-1}$, the droplet merging phenomenon would disappear. Under a large shear drag, the leading droplet would be pulled away from its micropore prior to 3.44 ms, but it could not catch the trailing droplet, which is also detached from its feeding source very quickly. Afterwards, the two droplets would move separately on the GDL surface in the gas channel. Results in

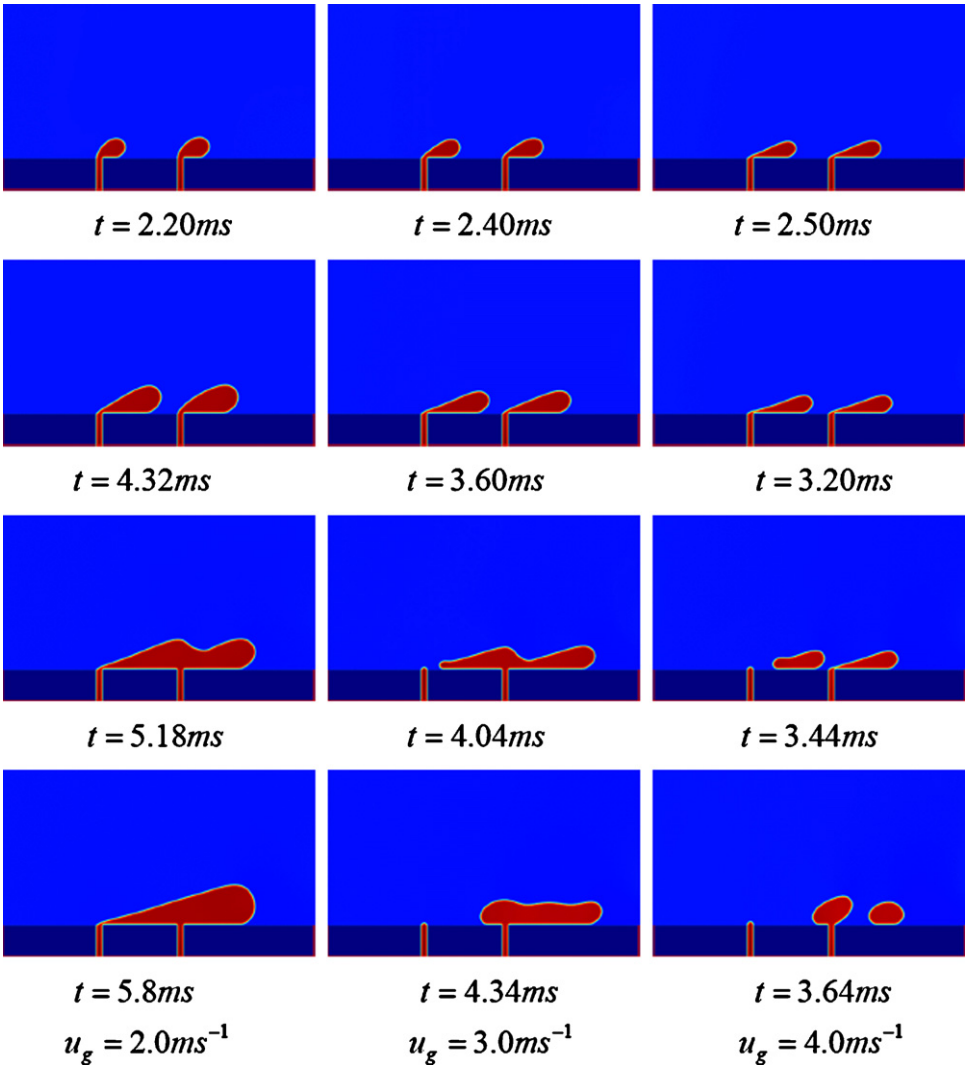


**Fig. 7.** Effects of inlet gas stream velocity on liquid droplet interaction.

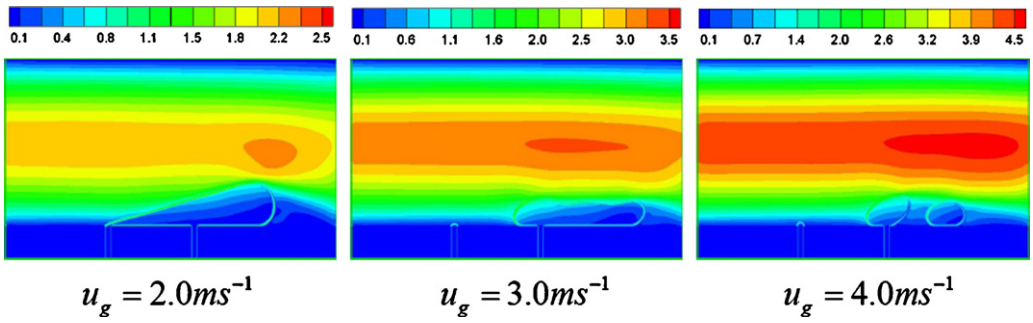


**Fig. 8.** Liquid droplet development and fluid velocity distribution.

Fig. 7 confirm that a high gas stream velocity is helpful to liquid droplet removal in a gas channel of a PEM fuel cell, which would in turn benefit the gas stream flows, as illustrated in Fig. 8.

Effects of the two micropores distance on liquid droplet interaction are next studied. In these three cases, the inlet gas stream velocity is specified at 4.0 m $s^{-1}$, while the pore distances are set at 200, 240, and 280 μm, respectively. Detailed simulation results are presented in Fig. 9.

At a relatively short distance of 200 μm, the leading droplet would be detached from its feeding pore under a strong shear drag from the gas stream, but comparing with the other two cases, its detaching time is slightly delayed by the close influence of the

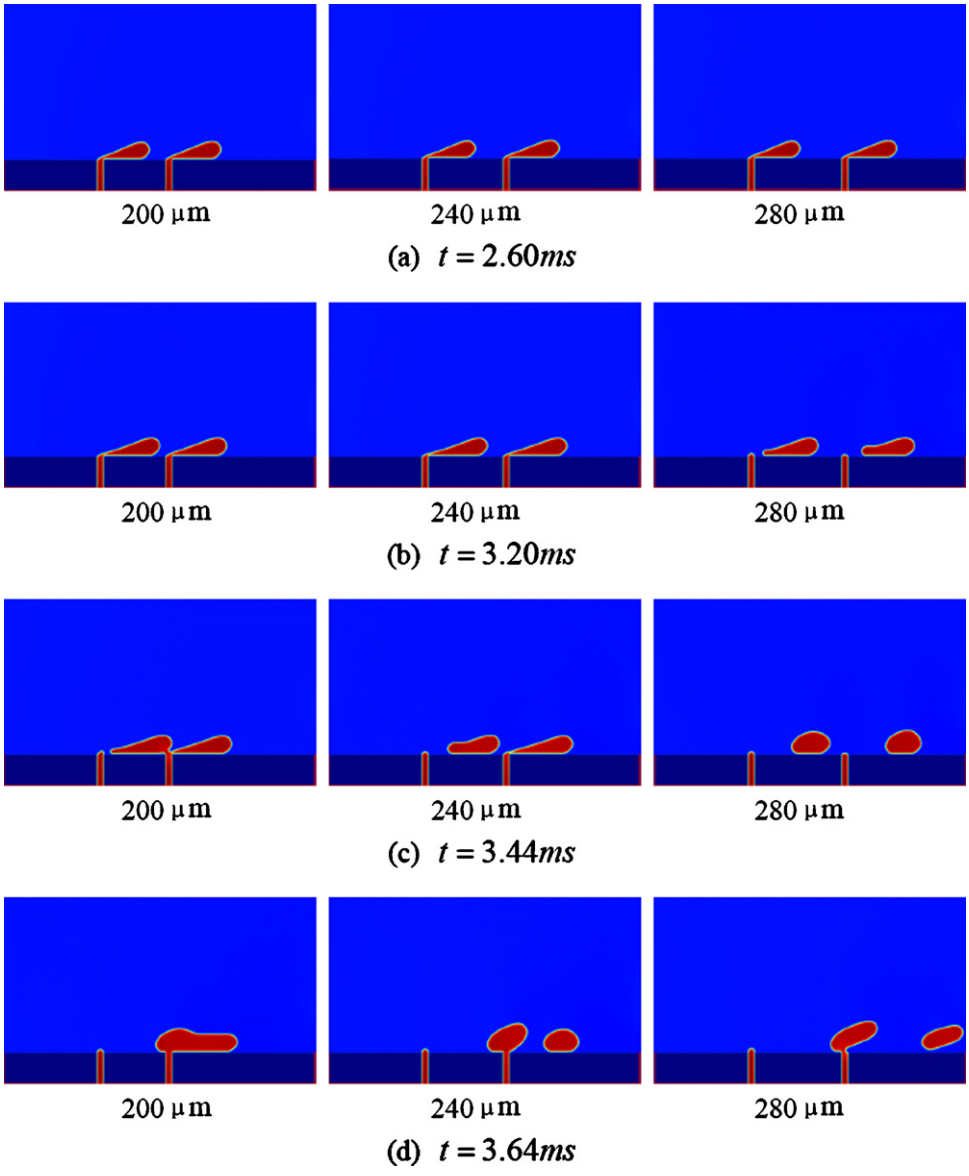


**Fig. 9.** Effects of micro pore distance on liquid droplet interaction.

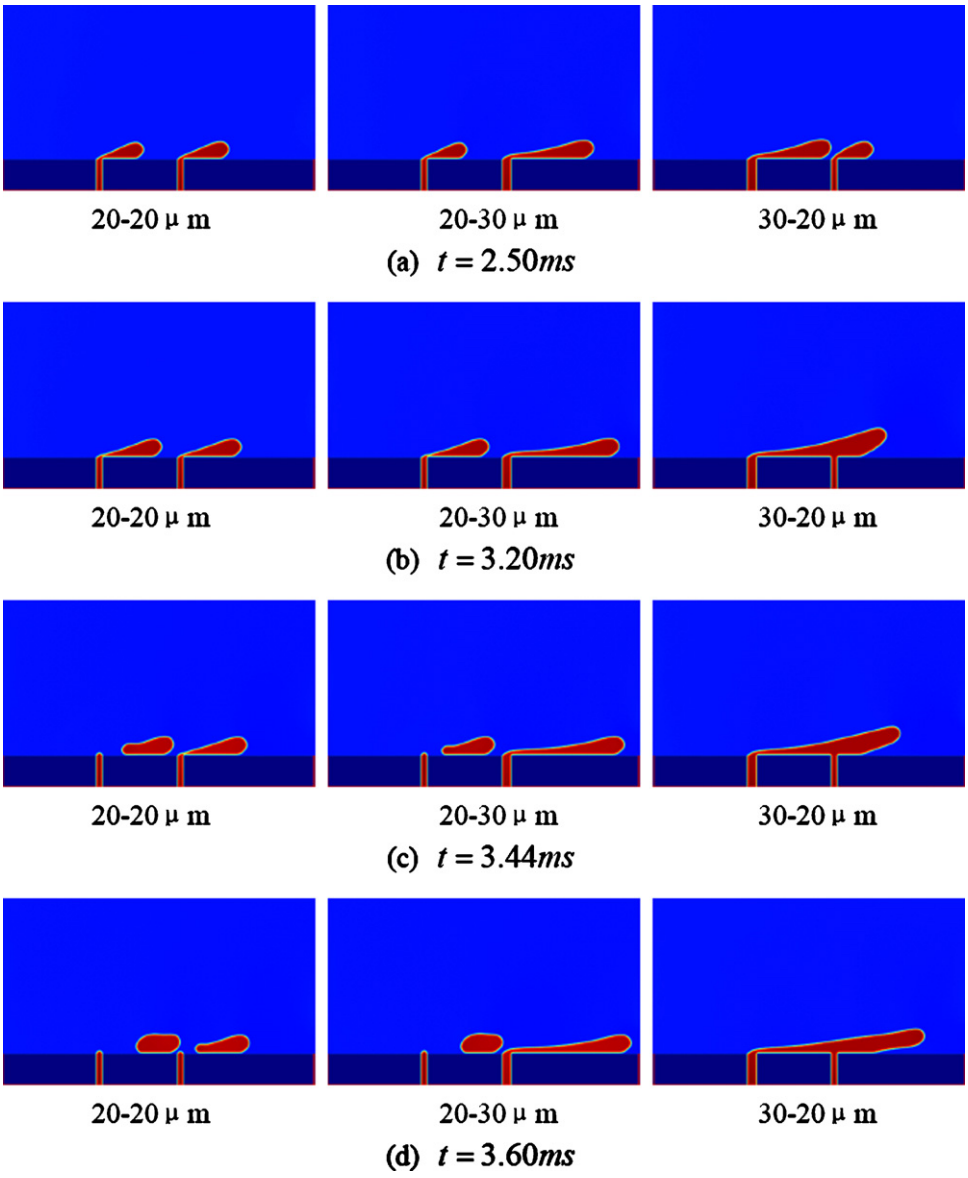


**Fig. 10.** Effects of different micro pore combinations on liquid droplet interaction.

second droplet. The leading droplet would exert strong influence on the trailing droplet by reducing the shear force it confronts. In this way, the leading droplet could catch up to and merge with the trailing droplet before latter is pulled away from the micropore.

As the pore distance is increased to 240 μm, the effect of the leading droplet on the trailing droplet becomes greatly weakened. As discussed earlier in Fig. 7, the trailing droplet, in this case, could be pulled away from its micropore soon after the leading droplet is detached. The two droplets would then move separately in the gas channel.

When the pore distance is further increased to 280 μm, interaction between the two droplets essentially disappears. As shown in Fig. 9, the two droplets would be detached at almost the same instant and behave independently in the entire process. This situation should be beneficial for liquid water removal and water management in a PEM fuel cell.

The pore size effects on liquid droplets interaction in a gas channel are also investigated in this paper. In the simulations, the inlet gas velocity is 4.0 m $s^{-1}$, the pore distance is set at 240 μm, but the two micropores are given different sizes. As shown in Fig. 10, one of the micropore is reduced to 20 μm, leading to different micropore combinations as 20-20, 20-30, 30-20, and 30-30. Results from the last 30-30 case have already been presented and discussed in Figs. 7 and 9.

Results from the 20-20 case are similar to those in the 30-30 case. The two droplets are initially elongated slightly along the flow direction. The leading droplet would then be pulled away from its feeding pore, but before it could collide with the trailing droplet, the second droplet would also become detached. During the entire simulation, the two droplets move separately in the gas channel.

For the 20-30 case in Fig. 10, the existence of the leading small droplet alters the shear force direction acting on the trailing large droplet, and consequently the trailing droplet is strongly stretched along the flow direction. Confronting a strong incoming flow, the small leading droplet could be easily detached from its micropore before the trailing large droplet could be pulled away. The two droplets would be able to merge thereafter.

With a large pore in front of a small one, droplet interaction would behave much differently. In the 30-20 case, the leading large droplet is more stretched than the trailing small droplet. The large and much-elongated leading droplet could easily touch the small trailing droplet and merge with it very quickly. During this process,

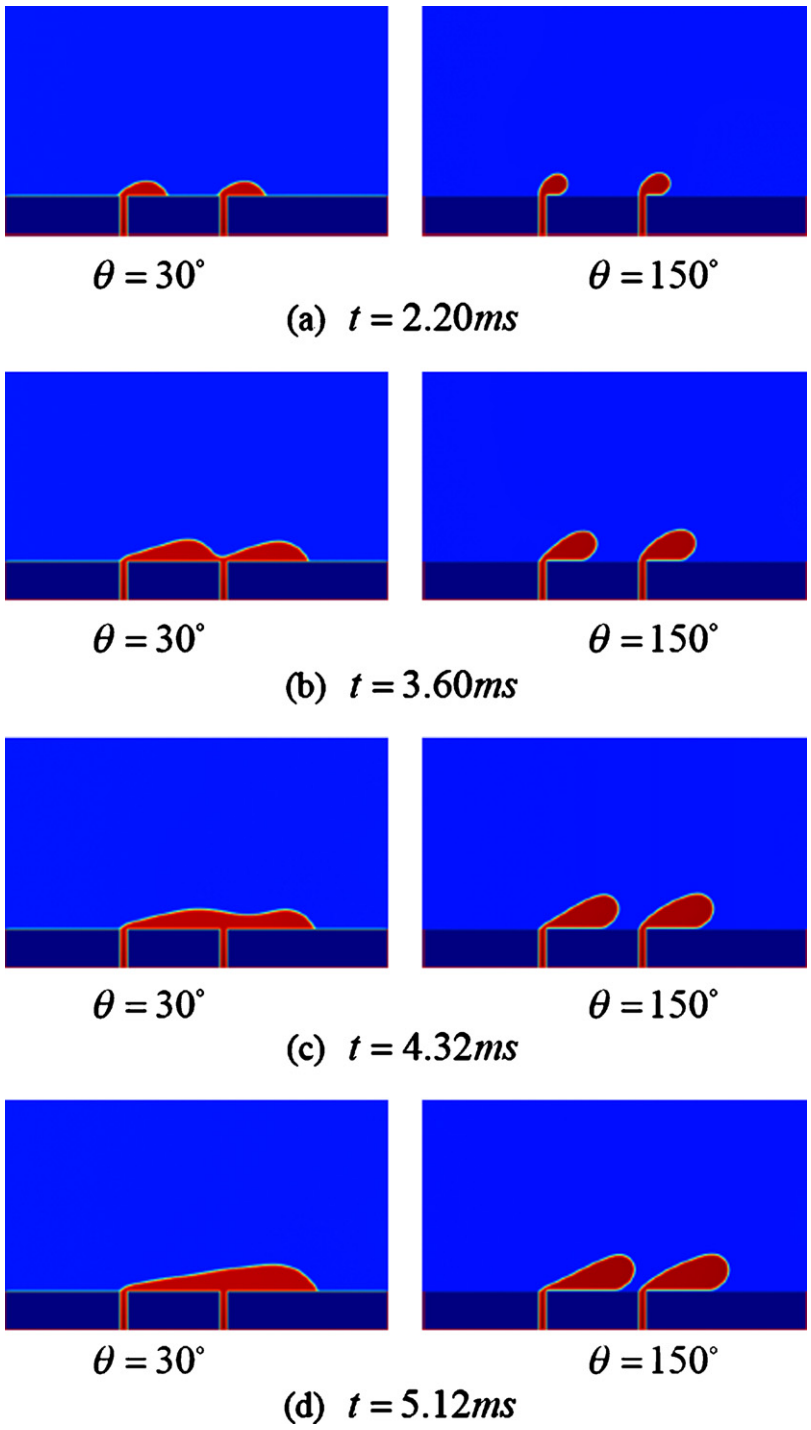


**Fig. 11.** Effects of surface contact angle on liquid droplet interaction.

however, both droplets cannot be pulled away from their feeding pores, and the merged liquid droplet becomes strongly stretched along the flow direction.

Results in Fig. 10 clearly show that different pore size combinations could exert significant influences on liquid droplet development in a gas channel. Placing two micropores with different diameters together would generally lead to enhanced droplet interaction, particularly with a large pore in front of a small one.

Effects of the GDL surface wetting property on liquid droplets development and interaction are finally simulated. In these cases, the inlet gas stream velocity is set at 2.0 m $s^{-1}$, while the pore distance is 240 μm.

The effect of a hydrophilic GDL surface with a contact angle of 30° on droplet interaction is illustrated in Fig. 11. With a hydrophilic surface, the two liquid water regions emerging from the micropores are closely attached to the channel wall as thin films, spreading along the flow direction. As a result, the two liquid regions could merge together very quickly, comparing with the hydrophobic cases in Figs. 7 and 11. The merged large liquid region remains attached to the feeding pores as a flat liquid film and becomes very difficult to eject.

For a hydrophobic GDL surface, liquid droplets behave differently with an increased GDL surface contact angle at 150°, comparing with the results in Fig. 7 with a contact angle at 120°.

As the surface contact angle increases, the interaction process between the two droplets becomes weaker, which is attributable to the interaction between the liquid droplet and solid wall. As such, liquid droplet removal may be enhanced by a more hydrophobic GDL surface.

Results in Figs. 7 and 11 indicate that a strongly hydrophobic GDL surface may decrease liquid droplet interaction, benefit liquid water removal, and consequently, improve water management in a PEM fuel cell.

## 5. Conclusions

In this paper, the Shan-Chen two-phase lattice Boltzmann model, along with the popular D2Q9 scheme, has been employed to simulate two liquid droplets development and interaction in a gas channel of a PEM fuel cell. The two-phase two-dimensional lattice Boltzmann model has been validated using two representative test cases concerning phase separation and liquid–solid interaction. In present numerical simulations, particular attention has been paid to the effects of a number of key influential parameters on liquid water droplet transport behaviors, including the gas flow velocity, initial droplet distance, different micropore combinations, and the GDL surface wetting properties.

Results confirm that an increased gas stream velocity and liquid pore distance may prevent liquid droplet interaction, enhance liquid droplet removal, and benefit water management in the gas channel of a PEM fuel cell. Numerical simulations further indicate that different pore size combinations may promote droplet interaction, particularly with a large pore in front of a small one. On the contrary, a more hydrophobic GDL surface can decrease liquid droplet interaction, benefit liquid water removal, and consequently improve PEM fuel cell water management. The present lattice Boltzmann simulations are intended to provide more details on liquid droplet interaction behaviors and enhance fundamental understanding of the related dynamic phenomena.

## Acknowledgement

This research work was financially supported by the National Natural Science Foundation of China (No. 10972197).

## References

[1] K. Tüber, D. Pócza, C. Hebling, J. Power Sources 124 (2003) 403.
[2] X.G. Yang, F.Y. Zhang, A.L. Lubawy, et al., Electrochem. Solid-State Lett. 7 (2004) A408.
[3] F.Y. Zhang, X.G. Yang, C.Y. Wang, J. Electrochem. Soc. 153 (2006) A225.
[4] A. Turhan, K. Heller, J.S. Brenizer, et al., J. Power Sources 160 (2006) 1195.
[5] P.K. Sinha, P. Halleck, C.Y. Wang, Electrochem. Solid-State Lett. 9 (2006) A344.
[6] D. Spernjak, A.K. Prasad, S.G. Advani, J. Power Sources 170 (2007) 334.
[7] I. Manke, C. Hartinig, M. Grunerbel, et al., Appl. Phys. Lett. 90 (2007) 174105–174113.
[8] A. Bazylak, D. Sinton, Z.S. Liu, et al., J. Power Sources 163 (2007) 784.
[9] D.S. Hussey, D.L. Jacobson, M. Arif, et al., J. Power Sources 172 (2007) 225.
[10] M.A. Hickner, N.P. Siegel, K.S. Chen, et al., J. Electrochem. Soc. 155 (2008) B427.
[11] W. He, J.S. Yi, T.V. Nguyen, AICHE J. 46 (2000) 2053.
[12] Z.H. Wang, C.Y. Wang, K.S. Chen, J. Power Sources 94 (2001) 40.
[13] L. You, H. Liu, Int. J. Heat Mass Transfer 45 (2002) 2277.
[14] T. Berning, N. Djilali, J. Electrochem. Soc. 150 (2003) A1589.
[15] N.P. Siegel, M.W. Ellis, D.J. Nelson, et al., J. Power Sources 128 (2004) 173.
[16] S. Shimpalee, S. Greenway, D. Spuckler, et al., J. Power Sources 135 (2004) 79.
[17] H. Meng, C.Y. Wang, J. Electrochem. Soc. 152 (2005) A1733.
[18] W.Q. Tao, C.H. Min, X.L. Liu, et al., J. Power Sources 160 (2006) 359.
[19] Y. Wang, C.Y. Wang, J. Electrochem. Soc. 153 (2006) A1193.
[20] H. Ju, G. Luo, C.Y. Wang, J. Electrochem. Soc. 154 (2007) B218.
[21] A.A. Shah, G.S. Kim, W. Gervais, et al., J. Power Sources 160 (2006) 1251.
[22] H. Meng, J. Power Sources 168 (2007) 218.
[23] H. Meng, J. Power Sources 171 (2007) 738.
[24] U. Pasaogullari, P.P. Mukherjee, C.Y. Wang, et al., J. Electrochem. Soc. 154 (2007) B823.
[25] H. Wu, P. Berg, X. Li, J. Power Sources 165 (2007) 232.
[26] K. Jiao, B. Zhou, J. Power Sources 175 (2008) 106.
[27] H. Ju, J. Power Sources 185 (2008) 55.
[28] H. Wu, X. Li, P. Berg, Electrochim. Acta 54 (2009) 6913.
[29] H. Meng, Int. J. Hydrogen Energy 34 (2009) 5488.
[30] H. Meng, B. Ruan, Int. J. Energy Res. 35 (2011) 2.
[31] H. Meng, Int. J. Hydrogen Energy 35 (2010) 5569.
[32] X.-D. Niu, T. Munekata, S.-A. Hyodo, et al., J. Power Sources 172 (2007) 542.
[33] J. Park, X. Li, J. Power Sources 178 (2008) 248.
[34] P.P. Mukherjee, C.Y. Wang, Q. Kang, Electrochim. Acta 54 (2009) 6861.
[35] P.P. Mukherjee, Q. Kang, C.Y. Wang, Energy Environ. Sci. 4 (2011) 346.
[36] P. Quan, B. Zhou, A. Sobiesiak, et al., J. Power Sources 152 (2005) 131.
[37] K. Jiao, B. Zhou, P. Quan, J. Power Sources 157 (2006) 226.
[38] L. Hao, P. Cheng, J. Power Sources 190 (2009) 435.
[39] X. Shan, H. Chen, Phys. Rev. E 47 (1993) 1815.
[40] X. Shan, H. Chen, Phys. Rev. E 49 (1994) 2941.
[41] M.C. Sukop, D. Or, Water Resour. Res. 40 (2004) W01509.
[42] H. Huang, Z. Li, S. Liu, et al., Int. J. Numer. Meth. Fluids 61 (2009) 341.
[43] X. He, G.D. Doolen, J. Stat. Phys. 107 (2002) 309.
[44] Y.H. Qian, D. D'Humières, P. Lallemand, Europhys. Lett. 17 (1992) 479.